Activation and Inactivation of Single Calcium Channels in Snail Neurons

A. M. BROWN, H. D. LUX, and D. L. WILSON

From the Department of Neurophysiology, Max-Planck-Institut für Psychiatrie, D-8000 München 40, Federal Republic of Germany, and the Department of Physiology and Biophysics, University of Texas Medical Branch, Galveston, Texas 77550

ABSTRACT Activation and inactivation properties of Ca currents were investigated by studying the behavior of single Ca channels in snail neurons. The methods described in the previous paper were used. In addition, a zero-phase digital filter has been incorporated to improve the analysis of latencies to first opening, or waiting times. It was found that a decrease in the probability of single channel opening occurred with time. This was especially marked at 29°C and paralleled the inactivation observed in macroscopic currents. The fact that a single channel was observed means that there is a significant amount of reopening from the "inactivated" state. Small depolarizations at 18°C showed little inactivation. From these measurements, histograms of single channel open, closed, and waiting times were analyzed to estimate the rate constants of a three-state model of activation. Two serious discrepancies with the model were found. First, waiting time distributions at −20 mV were slower than those predicted by parameters obtained from an analysis of the single channel closed times. Second, it was shown that the time and the magnitude of the peak of the waiting time histogram were inconsistent with a three-state model. It is concluded that a minimum of four states are involved in activation. Some four-state models may be eliminated from further consideration. However, a comprehensive model of Ca channel kinetics must await further measurements.

INTRODUCTION

In the preceding paper (Lux and Brown, 1984), it was shown that activation of whole cell Ca currents and membrane patch Ca currents proceeded along identical lines. Activation is not a Hodgkin-Huxley m^2 process and there was strong evidence that a linear, sequential, three-state model of activation did not fit the results either. Using data from patches containing single channels, the activation process is examined in more detail in the present paper. The waiting times until first opening were found to be distributed in a way not predicted by the three-state model. Inconsistencies with the three-state model were also reported by Hagiwara and Ohmori (1983). An additional finding was that the probability of opening of a single channel decreased at longer times. This is a direct demonstration of inactivation of Ca channels.

Address reprint requests to Dr. A. M. Brown, Dept. of Physiology and Biophysics, University of Texas Medical Branch, Galveston, TX 77550.

J. GEN. PHYSIOL. © The Rockefeller University Press · 0022-1295/84/05/0751/19$1.00

Volume 83 May 1984 751–769

METHODS

Most of the methods were described in the previous paper and additional methods related to data analysis are described here. A zero-phase digital filter was used to process the single Ca channel currents. We began to use this filter primarily because of our interest in the distribution of waiting times, i.e., the time from the beginning of a voltage pulse to the first channel opening. This distribution may be markedly affected by the types of analog filtering that are currently employed for single channel analysis. The problem that occurs is that filters with very good amplitude cut-off in the frequency domain also have

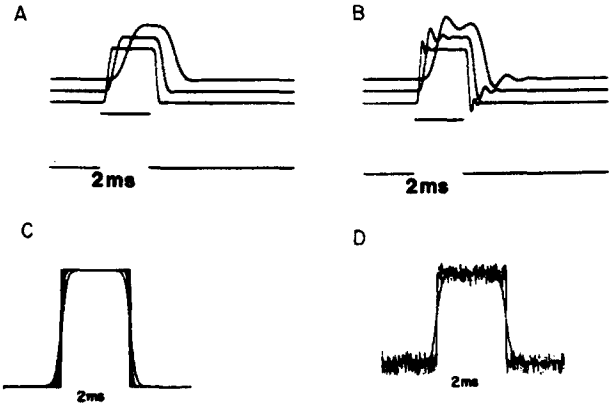

FIGURE 1. Pulse responses of analog filters and a zero-phase digital filter. (*A*) Below is the 2-ms pulse used as an input to the analog filter used in the "linear phase" or Bessel mode (eight-pole). Above are the responses with the filter cut-off (3-dB point) at 4, 2, and 1 kHz. "Delays" as measured to the time of half-maximum response were 0.27, 0.53, and 1.0 ms, respectively. (*B*) The analog filter is in the Butterworth or "flat amplitude" mode (eight-pole). Delays are 0.23, 0.44, and 0.84 ms with cut-off frequencies of 4, 2, and 1 kHz. Note that there is significant ringing in the pulse response of a Butterworth filter. (*C*) Pulse response of the zero-phase digital filter described in the text for 3-dB cut-off frequencies of 1, 2, and 4 kHz (eight-pole). Note that there is no apparent time shift of the response. (*D*) Pulse response of the zero-phase digital filter with noise present having a uniform amplitude distribution and with the 3-dB cut-off frequency at 1 kHz (eight-pole). The filtered and unfiltered responses are superimposed to illustrate that no time shifting occurs and that the original width of the pulse is maintained at half the maximum amplitude.

significant phase shifts. In the time domain, these phase shifts appear as a "phasic delay" in the pulse response, and this occurs at filter cut-off frequencies where the pulse response may be otherwise acceptable, i.e., the pulse may reach full amplitude. In Figs. 1*A* and *B* we show the pulse response for a commercially available analog filter (model 852; Rockland, Inc., Gilbertsville, PA). Using the time to half-maximum as a measure of the delay, we measured delays as long as 1 ms, as indicated in the figure legend, when filtering at 1 kHz. It is possible to configure this filter to have a 16-pole response; this would result in approximately twice the delay. There are various solutions to the problem. It would be possible to correct the distribution after it was measured if the pulse response of the filter were known, the detector level were known, and the single channel data were relatively

noise free. Another possibility would be to use matched filters on the current and voltage traces; the beginning of the voltage pulse would then be measured in the same manner that the channel openings are detected. The solution that we have chosen is simpler: it consists of using a zero-phase digital filter (Kormylo and Jain, 1974) that is implemented as discussed below. The zero-phase filter results in no time shifting of the signal, as shown in Figs. 1*C* and *D*. In addition to its zero-phase characteristic, the digital filter has other quite useful attributes. Since the filtering is done off-line, we can digitize the data at a high sampling rate and then choose a filtering scheme that gives a good signal to noise ratio yet still allows one to see fast activity in the trace. A by-product of this procedure is that since the anti-aliasing analog filter is set at a relatively high cut-off frequency of 5–10 kHz, the capacitive artifact will decay faster and may therefore reach the dynamic range of the A/D converter more quickly.

A zero-phase digital filter is quite easy to implement for fixed record length data. It consists of taking any available digital filter and passing it through the data in both the forward and backward direction. Kormylo and Jain (1974) also presented a method for longer lengths of data. We used a single-pole Butterworth filter that is applied repetitively to give any number of poles in the filter response. The single-pole Butterworth design allows one to avoid the "ringing" that would be present in a multiple-pole Butterworth filter, as is shown for an analog filter in Fig. 1*B*. In Fig. 1*C*, we show the pulse response of the digital filter. Note that there is absolutely no time shifting of the data. In Fig. 1*D*, we show the pulse response obtained in the presence of noise.

We have arranged our single channel data in the form of histograms such as those that are commonly employed. Histograms were plotted as the number of events in a time bin. In some cases we have plotted a "rest" bin, which includes the rest of the events occurring after the last bin. Single channel openings or closings, which occurred at the end of a trace, were discarded from the distributions.

Our methods for fitting the model-dependent probability density function (PDF) to the observed histograms take into account the fact that transitions of <300 μs in duration were excluded from the analysis. As an example of our approach, consider the open time distribution. Assuming a Markovian process with a single open state, the PDF is given by

$$P_D = \frac{1}{\tau} e^{-t/\tau} \tag{1}$$

where τ is a constant. The number of events expected in a bin at time t is given by

$$N_{BIN} = N_{TOT} \int_{t-\Delta t/2}^{t+\Delta t/2} P_D dt, \tag{2}$$

where N_{TOT} is the total number of events in the distribution and the integral extends across a bin of width Δt. Because of the limited frequency response of the measurement, the beginning of the histogram was truncated. The total number of events measured in the histogram, N_{MEAS}, is given by the following:

$$N_{MEAS} = N_{TOT} \int_{T_1}^{\infty} P_D dt, \tag{3}$$

where T_1 is the time where the beginning truncation ends. From Eqs. 1–3 we obtain the following working expression:

$$N_{BIN} = N_{MEAS}\, e^{T_1/\tau}[e^{-(t-\Delta t/2)/\tau} - e^{-(t+\Delta t/2)/\tau}]. \tag{4}$$

A similar expression was used by Dionne and Liebowitz (1982). In addition to the bins

described above, we allow a "rest" bin, which includes the rest of the events that have duration longer than a time T_2. The number in this bin is given by

$$N_{REST} = N_{MEAS}\, e^{T_1/\tau} e^{-T_2/\tau}. \quad (5)$$

Eqs. 4 and 5 are the equations that we fit to the data. Note that the only free parameter is the mean open time, τ.

Similar analyses can be applied to the other histograms normally obtained. The starting point is always the PDF, and the ones we use are given in Appendix A. In addition, in Appendix A we present an analysis of the identifiability of the rate constants of a three-state model. That is, we have examined what parameters may be uniquely obtained from the various histograms.

To fit the data to the model we used a nonlinear optimization routine that is a modified form of the Marquardt routine (Marquardt, 1963), as it appears in Bevington (1969). The number of unitary events was not as large as we might have wished. This is largely because the intervals between stimuli were long due to the slow inactivation process. Hence we used a variety of methods for estimating the goodness of fit. We used various objective functions such as unweighted least squares, weighted least squares, maximum likelihood, and a "robust" estimator (Jennrich and Ralston, 1979). As described by Jennrich and Ralston, the maximum likelihood estimator is easily implemented for the case of multinomial data using a "weighting" of each bin with the inverse of the model value there. With the latter three techniques, we constrained the weights attributed to a single point to be ≤ 1. This helps eliminate unreasonably large weighting of the bins in which very few events occurred. Each objective function gave slightly different estimates of the parameters of interest, as reported later. For the most part, the estimates were within a range that did not change the conclusions. We report standard deviations on the estimates as described by Jennrich and Ralston (1979). As pointed out by Jennrich and Ralston, standard deviations on the parameters should be regarded cautiously.

Additionally, we have not accounted for the fact that unresolved brief openings would tend to divide the longer closed times into shorter ones. Nor have we accounted for the fact that unresolved, brief closures would also change the open time measurements. Such effects are discussed by Dionne and Liebowitz (1982).

RESULTS

The characteristic activity of a single Ca channel when the potential is stepped from −50 to −5 mV is shown in Fig. 2. The random nature of the transitions is apparent, as is the repetitive nature of the discharge, although the frequency with which transitions occur is clearly greater during the first 25 ms. Some intervals among a sequence of repetitive openings may be very brief compared to others, giving rise to a bursting pattern of discharge (Fenwick et al., 1982; Brown et al., 1982; Hagiwara and Ohmori, 1983).

At a lower temperature the number of openings early in the trace is clearly reduced (Fig. 3), although later in the trace the number of transitions seems to be similar to those observed at higher temperatures. The summed currents at the bottom of the figure reflect these differences.

Of interest in Fig. 2 is the fact that apparent inactivation occurs in the average of the patch currents. This occurs despite the fact that no outward currents were observed and no change in unitary amplitude took place. This is direct evidence that Ca channels inactivate because of a decrease in the probability of opening.

As discussed in the preceding paper (Lux and Brown, 1984), the patch contained a single channel because there were no simultaneous openings. Assuming that we have measured activity from a single channel, the openings later in the pulse are from recurrent openings of the same channel. This indicates that the process decreasing the probability of channel opening, which we have called inactivation, is not due to an absorbing state. The channel can return from this state. Of additional interest is the fact that inactivation is apparent in Fig. 2 at 28°C but

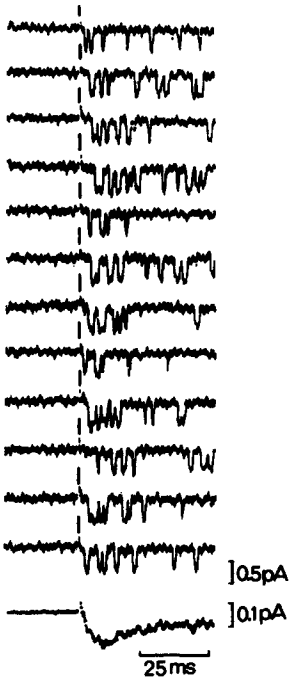

FIGURE 2. Patch recording of a single Ca channel at 28°C following a step depolarization from −50 to −5 mV. The time of the voltage step is indicated by the vertical line. The linear components of capacitive and leakage currents were removed by subtraction of the current response to a hyperpolarizing pulse of equivalent amplitude as described in the preceding paper. Below are averaged patch currents from 68 recordings. Note that the averaged current shows a tendency to "inactivate."

not in Fig. 3 at 9°C. Similar results are shown in Fig. 12 of the preceding paper. This effect of temperature qualitatively agrees with results from whole cell currents (Fig. 2 of the preceding paper) and is another way in which patch recordings agree with whole cell measurements.

There were relatively few times when there were no channel openings, or failures, during the voltage clamp pulses. In the experiment of Fig. 2, there were no failures at 28°C. The absence of any apparent inactivation in the average current from the single channel measurements at 9°C argues that the 15 failures

out of 72 trials in this case (Fig. 3) were not due to an independent inactivation process. The failures that occur at 9°C are more likely due to the finite length (50 ms) of the record. This conclusion is confirmed by the results in Fig. 12 of the previous paper, in which data from 200-ms pulses were obtained. Only one failure occurred in 49 records at 9°C and none occurred at 28°C.

Because of the difficulty in obtaining large numbers of records on the same patch, we decided to investigate the voltage dependence of inactivation in the following manner.

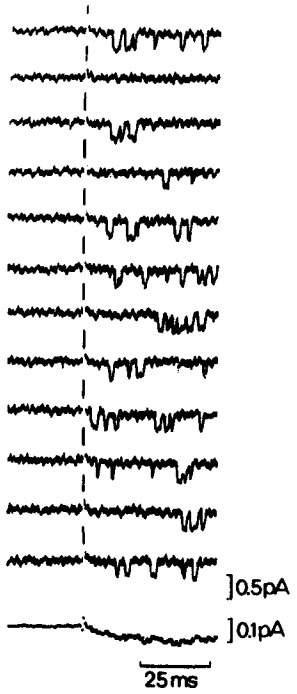

FIGURE 3. Patch recording under the same conditions as in Fig. 2 except that the temperature has been reduced to 9°C. Note that the channel openings early in the trace are much less frequent here than in Fig. 2. Also note that the average current shows that turn-on has been significantly slowed as was found for macroscopic currents at 0°C (Fig. 3 of preceding paper). Average current from 72 recordings.

In Fig. 4 the probability of channel opening was averaged across the first 50 ms and across an entire 400-ms pulse; both were then plotted against potential. This time-averaged probability of the channel being open was calculated as the fraction of the length of the trace in which the channel was open. Using 30 single channel records, the fractional open times averaged for the first 50 ms were compared with the fractional open times averaged over the entire record. The average values of the latter were found to be smaller at potentials above −5 mV. This result is consistent with the inactivation that occurs in whole cell currents at higher potentials at room temperature. The mean open times were

similar for the two sets of data, as were the average numbers of openings per burst. The relationship between P_o and potential was similar to that between normalized whole cell tail currents measured at −50 mV following steps to prepulse potentials over the same range (Brown et al., 1983).

Histograms of Channel Activity

In Fig. 5 we have plotted the histograms normally obtained from analysis of single channel data. Unitary activity was measured in 25 records of 350 ms duration at −20 and 0 mV. In previous work a three-state model of activation was used (Fenwick et al., 1982; Brown et al., 1982). We have also used the same model to present the single channel kinetics in more detail than we had done previously. In the kinetic scheme below we assume voltage-dependent rate

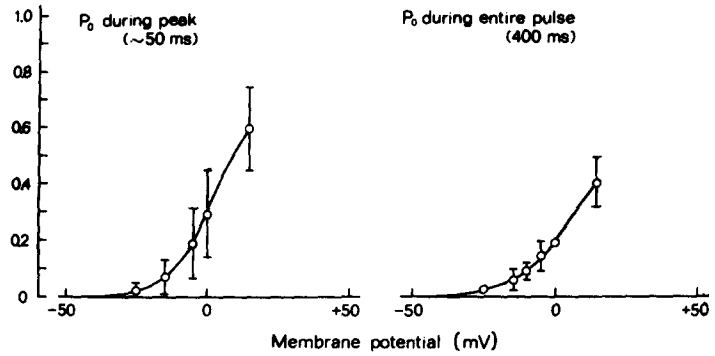

FIGURE 4. The probability of opening, P_o, as a function of potential. The values were computed from records that had evidence of only one active channel. The number of records, n, per data point, ranged from 4 to 20. The P_o values were estimated on the left-hand side as the fraction of time that the channel was open over a period of 50 ms, and on the right-hand side, as the same fraction over the total record length of 400 ms. The P_o-V relationship is similar to the relationship between the normalized amplitude of tail currents recorded at a return potential of −50 mV and the potential during the preceding command step (Brown et al., 1983).

constants. We let R, A, and O stand for "rest," "activated," and "open" states, respectively, and we are interested in the probability of transitions between these states.

$$\mathrm{R} \underset{k_{-1}}{\overset{k_{+1}}{\rightleftharpoons}} \mathrm{A} \underset{k_{-2}}{\overset{k_{+2}}{\rightleftharpoons}} \mathrm{O} \tag{6}$$

The distributions of the open times were described by a single exponential function and the open time histograms at two potentials are shown in Fig. 5. The number of openings was much less at −20 mV compared with 0 mV. The data were fit according to Eqs. 4 and 5 and the mean open times were 1.6 and 1.4 ms at −20 and 0 mV, respectively. Over the range of −20 to 0 mV, at 5-mV increments, there was little voltage dependence of the mean open time. Further-

more, the mean open time did not appear to be affected greatly by cooling, as described in the previous paper.

Single channel activity shows very brief closed times and much longer closed times as seen in Figs. 2 and 3 (see also Lux and Nagy, 1981; Fenwick et al.,

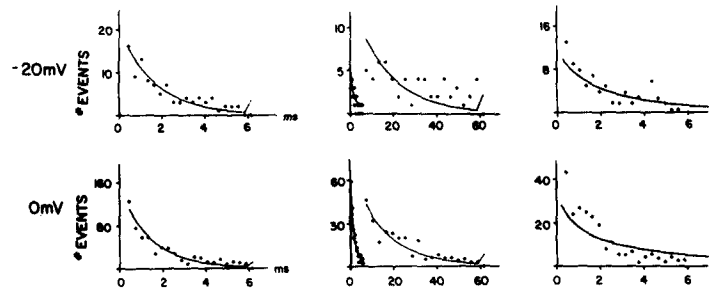

FIGURE 5. Open time (left), closed time (middle), and burst length (right) of histograms of single channel data obtained at −20 and 0 mV. Temperature was 18°C. Data points are plotted in the center of the bins. In the case of the open time and burst duration plots the bin widths are 0.3 ms. The closed time histogram is plotted with bin widths of 0.3 and 3 ms to try to illuminate the two phases in the decay of the data, and the change in bin width causes the discontinuity in these plots. The first bin, combining openings of ≤300 μs, is truncated in each plot because of the finite response time of the clamp. Actual transitions in this bin were excluded from the fitting as described in the Methods. In the case of the open and closed time histograms the last data point is a "rest" bin, which includes all of the rest of the data with longer intervals as described in Methods. Smooth curves in the plots are obtained from a three-state model. The open time histograms were fit with Eqs. 4 and 5 as described in the text using a least-squares objective function. The closed time histograms were fit using Eq. A1. From these two histograms all parameters in the model were identified, and the prediction for the burst length data is plotted using Eq. A9. Parameters in units of 1/ms at −20 mV are $k_{+1} = 0.17 \pm 0.04$, $k_{-1} = 0.37 \pm 0.09$, $k_{+2} = 0.19 \pm 0.03$, and $k_{-2} = 0.60 \pm 0.02$; the numbers of events measured were 89 and 96 for the closed time and open times, respectively; and the corresponding total numbers of events after extrapolation to time zero were 94 and 115. Parameters at 0 mV are $k_{+1} = 0.13 \pm 0.02$, $k_{-1} = 0.35 \pm 0.05$, $k_{+2} = 0.40 \pm 0.03$, and $k_{-2} = 0.70 \pm 0.05$; the number of events measured were 563 and 592 for the closed and open times, respectively; and the corresponding total numbers of events after extrapolation to time zero were 630 and 728. The time constants in milliseconds, computed from the k's above given in the order of the open τ, the faster closed τ, the slower closed τ, the faster burst duration τ, the slower burst duration τ, the faster macroscopic relaxation τ, and the slower macroscopic relaxation τ are 1.67, 1.5, 21, 1.1, 4.0, 1.0, and 2.7 at −20 mV and 1.43, 1.23, 16, 0.8, 1.6, 0.7, and 3.1 at 0 mV. These calculations were carried out using the full expressions for the various time constants as they appear in the text.

1982; Brown et al., 1982). Consistent with this observation are the two clear phases in the decay of the closed time histograms (Fig. 5). The closed time histograms were fit with equations similar to Eqs. 4 and 5, derived from the PDF in Appendix A, Eq. A1. In Appendix A we show that the rate constants k_{+1}, k_{-1},

and k_{+2} are uniquely identifiable from the closed time histogram. Fits to the data are shown in Fig. 5, and parameter estimates are given in the figure legend. At −20 mV the number of events was small and there is some uncertainty about fitting the distributions with exponential functions. But the patterns were similar to those obtained with the much larger numbers present at 0 mV. We should note that the distribution of open times is biased toward longer values because the briefest closures may not be resolved because of bandwidth limitation. A similar problem occurs when unresolvable brief openings interrupt closed times.

Bursts were identified as openings separated by short gaps; these groupings in turn were separated from each other by very much longer intervals. This resulted in the biexponential distribution of closed times. Bursts were defined then as repeated openings separated from other openings by periods three or more times the fast time constant of the closed time histogram. This definition included single openings. The distribution of burst durations is shown in Fig. 5. As described in Appendix A (Eq. A9), the apparent burst length is expected to be biexponentially distributed, and the parameters k_{-1}, k_{+2}, and k_{-2} should be uniquely identifiable from the data. In the case of our Ca data, bursts are not always clearly demarcated. Because of the somewhat arbitrary nature of defining a "burst" length and the fact that we truncated the bursts at 6 ms, we did not try to identify parameters from this distribution. Instead we used the parameters already identified above to predict a burst length distribution, and the predicted curves are shown in Fig. 5. This fit was fairly good, and there were no free parameters in the predicted curve.

Several other parameters can be calculated using the rate constants given in the legend to Fig. 5, and these are compared here to the appropriate experimental measurements. The average number of openings per burst was measured directly and in seven patches average values of 1.29 ± 0.20 and 1.51 ± 0.31 openings per burst were found at −20 and 0 mV, respectively. The predicted value for openings per burst is given by $1 + k_{+2}/k_{-1}$, and the values were 2.2 at 0 mV and 1.5 at −20 mV. The calculated probability of opening is easily obtained from Eq. 6, and it was 0.13 at 0 mV and 0.09 at −20 mV. These values are less than the usual values measured directly from the data, and this may be another clue that the three-state model is insufficient. The fast time constant in the closed time distribution, calculated from Eqs. A2 and A3, had a value of 1.23 ms at 0 mV and 1.5 ms at −20 mV. These latter values may be compared to values calculated from the approximate method used by Fenwick et al. (1982) given by $(k_{-1} + k_{+2})^{-1}$, which were 1.33 ms at 0 mV and 1.78 ms at −20 mV. The two time constants for the current relaxations and noise spectra are obtained from the eigenvalues of the matrix equation associated with Eq. 6 and they are given by

$$\tau_{1,2}^{-1} = 0.5\,[b \pm (b^2 - 4c)]^{1/2} \tag{7}$$

where

$$b = k_{+1} + k_{+2} + k_{-1} + k_{-2} \tag{8}$$

and

$$c = k_{-1}k_{-2} + k_{+1}k_{-2} + k_{+1}k_{+2} \quad (9)$$

(Lowry and John, 1910; Colquhoun and Hawkes, 1977). They were calculated to be 0.7 and 3.1 ms at 0 mV and 1.0 and 2.7 ms at −20 mV; these values are within the range of the noise values measured experimentally (Table II, Lux and Brown, 1984), although the tail current τ's tend to be much faster (Table II, Lux and Brown, 1984; Brown et al., 1983). The difference may arise from missed fast openings and closures.

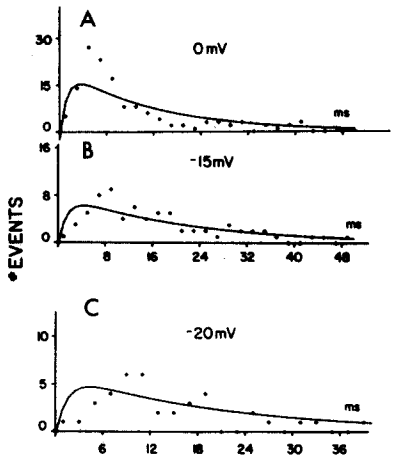

FIGURE 6. Waiting times at different potentials. (*A* and *B*) Waiting time histograms are shown at 0 and −20 mV from a single experiment. The experiments were done at room temperature with pulse durations of 50 ms. The smooth curves in both cases were obtained using Eq. A8 and the parameters for a three-state model as found in Fig. 5. The number of measurements at 0 mV was 151 with 12 failures, and at −20 mV the number of measurements was 81 with 9 failures. The computed curves were obtained by multiplying the PDF integrated across the time bin by the total number of records including the failures. The presence or absence of the failures does not affect the position of the peak. Note that at −20 mV the predicted curve from a three-state model is somewhat "faster" than the measured response. (*C*) Waiting time histogram from another cell at −20 mV using 40-ms pulses. The smooth curve is from the same model and parameters as in *B*. The number of measurements was 62 and the number of failures was 24.

Latencies to First Openings

The distributions of the latencies to first openings, or waiting times, are shown in Fig. 6. The openings came from a single channel, as deduced from arguments presented earlier. Two distributions of waiting times taken from the same patch at −20 and 0 mV are shown in *A* and *B*, and *C* shows additional measurements at −20 mV from another patch. The presence of both a rising phase and a falling phase in the data is evidence of an additional electrically silent state between the "rest" and "open" states. Adjoining states would require the absence of a preceding rise.

The smooth curve plotted on the histograms is the waiting time predicted

from parameters estimated in Fig. 5. Note that in each case the peak is larger than the predicted response and occurs later. Thus, the waiting time measurements are somewhat "slower" than the waiting time predictions based on the two closed time measurements. This indicates that the waiting time data may emphasize different kinetics than the closed time data, which were obtained continuously along the voltage clamp pulse. We suggest that there is an additional state in the activation process that has been uncovered by the waiting time measurements.

There is a possible source of error in the above analysis. Inactivation was present at 0 mV; thus, kinetic parameter estimates were corrupted by this in a manner to make the closed times longer. These longer values in turn act to delay the peak predicted by the three-state model. At −20 mV there was no inactivation (see Fig. 4), which should simplify the analysis. These arguments may explain why there is less discrepancy between the times to the measured and predicted peaks in Fig. 6*A* than in Figs. 6*B* and *C*.

As shown in Fig. 7, the waiting time is greatly prolonged at a lower temperature (compare also Figs. 2 and 3). In addition, a relatively large number of records showed no openings in this relatively short pulse, although with 200-ms pulses there was only one failure in 49 records at 9°C. Thus, many first openings may occur quite late. These results are consistent with observations in over 50 experiments that the turn-on of the macroscopic currents is greatly prolonged by decreases in temperature (Lux and Brown, 1984; Brown et al., 1983).

As discussed above, we found that the peaks of the waiting time histograms did not match those predicted from steady state measurements. Next, we tried to fit these data with Eq. A8. We found that the fits failed near the peaks, and that the two ρ values tended to be almost equal, i.e., there was only one value for ρ. The ρ values in Eq. A8 are the eigenvalues for the system of differential equations describing the three-state model with an absorbing open state. The closed time PDF is obtained from this system of differential equations and has the same system eigenvalues. The only difference in analyzing the closed time or waiting time, as opposed to the complete system, is the initial condition applied to the system of equations. Experimentally we determined that the waiting time ρ's tended to be equal, and thus were clearly discrepant with the reciprocal time constants obtained from the closed time data.

These results led us to investigate the relationship between the time of the peak and the size of the peak of the waiting time PDF for a three-state, sequential model as described in Appendix B. The analysis indicates that it is impossible to reconcile the waiting time measurements with a three-state model. First, in Fig. 8*A* we have plotted the magnitude of the peak, $f(\rho)$, vs. ρ at a constant time to peak of 1 ms. An amplitude found on this curve will normally be associated with 2 ρ values as was described previously. However, there is a maximum in this curve and only a single ρ value is obtained there. This explains why we tended to obtain similar ρ values with the relatively "large" measured peaks. Also, we found that our measured peak waiting times often fell above the maximum value in a plot such as that in Fig. 8*A*. Thus, in Eq. B8 we present an expression relating the maximum permissible value for the peak of the PDF, $P_{RO}{}^*(t_p)$, and

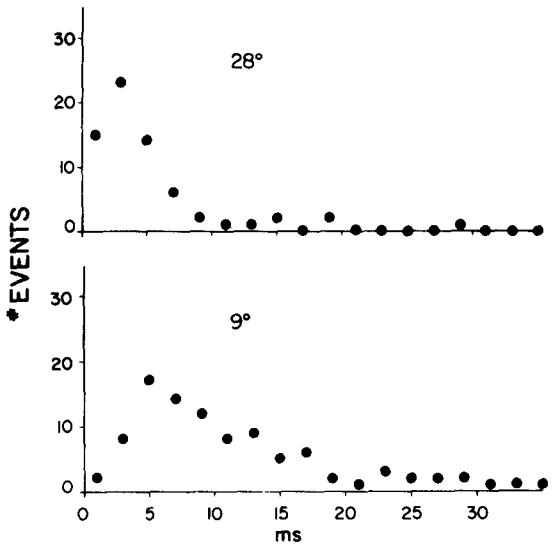

FIGURE 7. Effect of temperature on the waiting time histogram at −5 mV. The number of measurements was 68 at 28°C and there were zero failures. The number of measurements at 9°C was 72 and there were 15 failures. Records were 250 ms in length. Note that with the decrease in temperature there is a marked "slowing" and broadening of the waiting time distribution.

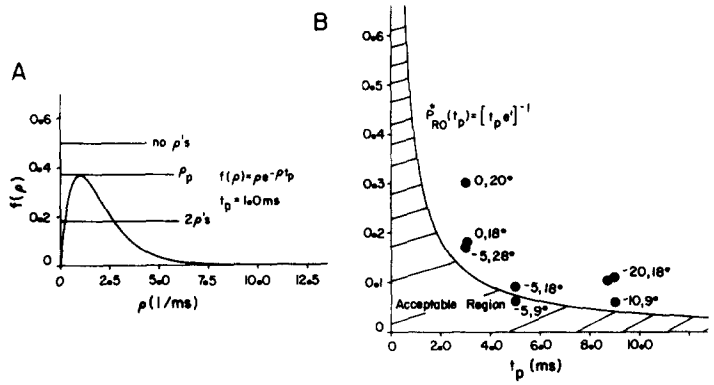

FIGURE 8. (*A*) The solid line is a plot of the maximum value of the waiting time PDF given by $f(\rho)$ defined in Eq. B5. The time of peak was set at 1.0 ms. Given a t_p of 1.0 ms and a maximum value of the PDF corresponding to one of the three horizontal curves, we find either two distinct ρ values, a repeated ρ value, or no permissible ρ values. (*B*) The smooth curve is the maximum allowable value of the peak of the waiting time PDF as a function of t_p from Eq. B8. Measured values for a three-state model must lie in the "acceptable region." The ordinate shows the maximum probability density (1/ms). Potential and temperature are indicated. All but one of the data points lie in the "forbidden zone."

the time of peak, t_p. This equation is plotted in Fig. 8*B* and there we have indicated an "acceptable" region where the data points must lie in order to be consistent with a three-state model. Note that all but one of the data points lie outside the acceptable region, giving us a second inconsistency with the model. Moreover, one source of error would make the discrepancy larger, which is that peak values were taken from histograms of the data with finite bin widths; such values would tend to be smaller than the true peak values.

DISCUSSION

The bursting behavior of single Ca channels and the biexponential nature of the closed time histogram has led to a three-state model of activation as an explanation (Fenwick et al., 1982; Brown et al., 1982). The rate constants of such a model gave results that were consistent with the two relaxation τ's measured for the turn-off of whole cell Ca currents and with the two corner frequencies shown by noise spectra. Inconsistencies occur when the distribution of latencies to first opening or waiting time is considered. Moreover, in whole cell current measurements, we previously reported that the τ's fitting the tail currents did not adequately account for the delay in the turn-on currents (Brown et al., 1983). Also, cooling had a much larger effect on turn-on than on turn-off at comparable potentials.

In the present paper we have concentrated to a large degree on the waiting times. These were measured accurately in the present experiments because phasic delay caused by filtering was avoided. The zero-phase digital filter allowed us to resolve the channel openings at bandwidths that ordinarily might produce serious delay.

The measured waiting times tended to be "slower" than the waiting time distribution predicted from parameters obtained from a three-state model as applied to the closed time data measured throughout the record (Fig. 6). Note that this was true at −20 mV and at 19°C, conditions in which inactivation was minimal or not present in either whole cell or averaged patch clamp currents. Such a consideration is important because inactivation would complicate the closed time histogram. In all but one case the peak and the time of peak of the waiting time PDF fell outside the acceptable region for the three-state sequential model (Fig. 8*B*). These results and the results of the macroscopic current experiments should be incorporated into a model of Ca current activation that requires, as a minimum, four states rather than the minimum three states proposed previously. Along these lines, Hagiwara and Ohmori (1983) have recently suggested that activation of Ca channels cannot be accounted for by a three-state model on the grounds that the faster of the two time constants from a closed time histogram is much less potential dependent than the slower time constant. They indicate that this result is inconsistent with the manner in which the two time constants depend on the rate constants in the closed time PDF of a three-state model. Their latency histograms showed potential dependence but were inconclusive in regard to their compatibility with the closed time PDF. As an alternative, Hagiwara and Ohmori (1983) proposed the following scheme:

$$\text{closed}_1 \underset{k_{-1}}{\overset{k_{+1}}{\rightleftharpoons}} \text{closed}_2 \underset{k_{-2}}{\overset{k_{+2}}{\rightleftharpoons}} \text{open} \underset{k_{-3}}{\overset{k_{+3}}{\rightleftharpoons}} \text{closed}_3. \tag{10}$$

We have found several inconsistencies with this scheme. First, assuming closed_1 to be initially filled when the membrane is at rest, this scheme gives the same waiting time distribution prediction as a three-state model. Thus, our analyses above would also apply to this model, particularly the results in Appendix B, and it would suffer from the same deficiencies. Note that the assumption that closed_1 includes all of the channels at rest is not arbitrary. If closed_2 or closed_3 were to include some channels at rest, then one would not see an initial delay in the turn-on of macroscopic Ca current. This follows from the differential equation describing the probability of being in the open state, i.e.,

$$\frac{d(\text{open})}{dt} = -(k_{-2} + k_{+3})(\text{open}) + k_{+2}(\text{closed}_2) + k_{-3}(\text{closed}_3). \tag{11}$$

Immediately after initiation of a voltage clamp step, the probability of being in the open state is zero, and because a delay is observed, the first derivative of this probability is also zero. It follows from Eq. 11 that closed_2 and closed_3 must therefore be zero, and the argument is complete. The remaining arguments have to do with expectations from macroscopic currents. As a result of the closed_3 state having a fairly fast kinetic exchange with the open state, we would expect a rising phase in the tail currents. But this has not been observed (Fenwick et al., 1982; Brown et al., 1983; Lux and Brown, 1984). Additionally, the voltage dependence of the steady state activation parameter, as measured by tail current amplitudes, might be expected to pass through a maximum. Again, this was not observed (Brown et al., 1983). Another four-state model is one in which three closed states precede the open state. Such a model has been proposed to explain macroscopic Ca current (Brown et al., 1983), but the single channel data have not yet been incorporated into this scheme.

Cooling may slow transitions from the first closed state of a minimal four-state model (or earlier steps in higher-order models). Thus, turn-on of macroscopic currents is more affected than turn-off and waiting time and slow closed times are more affected than open times or fast closed times. This may indicate that a metabolic process modulates an early transition. Cachelin et al. (1983) have recently shown that cAMP increases the opening probability of Ca channels and this could be related to our observations. Metabolic regulation of channel density is also possible, but it would not explain the kinetic effects we observed on macroscopic and single channel currents.

The foregoing interpretation neglects transitions to the inactivated state. However, a complete kinetic scheme for Ca channels must include inactivation. A long-standing sore point in the Ca current literature is whether inactivation is due to contamination from outward currents that are either Ca or non-Ca related. The reduction in P_o at longer times at potentials above −5 mV is proof of an inactivation process that occurs as a result of a decreased probability of channel opening. We wish to point out that the reason that we have found evidence of inactivation in patch currents, whereas other investigators have not

(Fenwick et al., 1982; Hagiwara and Ohmori, 1983), has to do with our experimental conditions. We used Ca rather than Ba (see Fig. 4 of the preceding paper), and we have done experiments at room temperature or above, where inactivation of macroscopic Ca currents (Y. Tsuda and A. M. Brown, unpublished observations; and Fig. 12 of the preceding paper) and patch currents (compare Figs. 2 and 3 and Fig. 12 of the preceding paper) is much greater. Reuter et al. (1982) observed inactivation of multichannel patch clamp Ba currents during 1-s depolarizations and after depolarizing patch prepulses of unspecified duration. In their case, complete inactivation was observed, although in most circumstances voltage-dependent inactivation of Ba currents is usually far from complete (Brehm and Eckert, 1978; Brown et al., 1981).

Of additional interest is the fact that the Ca channels reopen following a closure in what might be thought of as an inactivated state; that is, there are some fairly long closed times in records in which the inactivation is present in the averaged patch current. A biexponential time course of inactivation of macroscopic Ca currents has been described (Brown et al., 1981) with one very slow component, and the time course for recovery of macroscopic currents is also at least biexponential with full recovery requiring as long as 10 s (Yatani et al., 1983). The decreased probability of opening that we have observed in the presence of inactivation coincides with the fast inactivation process. The macroscopic currents may be completely inactivated by a slower process, which implies that unitary activity would cease in a sufficiently long record.

The question as to whether inactivation is coupled to or independent of activation remains open. For Ca current-dependent inactivation, coupling is obligatory. Sodium channels at comparable levels of activation show many more nulls (Patlak and Horn, 1982; D. L. Kunze and A. M. Brown, unpublished observations). For the sodium system, inactivation is treated as an independent process, although coupling certainly has its adherents. The comparison might favor a coupled model for Ca channels where nulls would never occur. However, the fact that inactivation is not completely absorbing on the time scale of our experiments leaves open the possibility that the two processes are independent for Ca channels as well.

APPENDIX A

Identifiability Analysis Applied to the PDFs of a Three-State Model

Before undertaking a parameter estimation problem, the identifiability of the parameters must be examined. As we will demonstrate, the rate constants of interest are uniquely identifiable from open time, closed time, and burst length PDFs but not from the waiting time PDF. Identifiability concepts have normally appeared in systems theory analysis and compartmental analysis (for recent reviews see R. F. Brown, 1980; Cobelli and DiStefano, 1980). We have analyzed the PDFs normally obtained for a three-state, sequential model (Eq. 6). In terms of an identifiability analysis, the most interesting PDF is the closed time PDF as given below (Colquhoun and Hawkes, 1981):

$$P_{CI}(t) = \frac{k_{+2}}{\rho_4 - \rho_3}\left[(k_{+1} - \rho_3)e^{-\rho_3 t} + (\rho_4 - k_{+1})e^{-\rho_4 t}\right] \tag{A1}$$

where

$$\rho_3,\ \rho_4 = 0.5[b + (b^2 - 4c)^{0.5}] \tag{A2}$$

and

$$\begin{aligned} b &= k_{+2} + k_{+1} + k_{-1} \\ c &= k_{+2}k_{+1}. \end{aligned} \tag{A3}$$

Eq. A1 can be written in the following form:

$$P_{\mathrm{Cl}} = Ae^{-\rho_3 t} + Be^{-\rho_4 t}, \tag{A4}$$

where A and B can be obtained by inspection. Consider that we could fit the data to Eq. A4 and obtain A, B, ρ_3, and ρ_4. The identifiability analysis then consists of determining if we can obtain a unique set of parameter values, k_{+1}, k_{-1}, and k_{+2} from A, B, ρ_3, and ρ_4 using the available equations. From the expressions for A and B we obtain

$$k_{+1} = \frac{A\rho_4 + B\rho_3}{B + A}. \tag{A5}$$

Other results quickly follow and we obtain

$$k_{+2} = \frac{A(\rho_4 - \rho_3)}{k_{+1} - \rho_3} \tag{A6}$$

and

$$k_{-1} = (\rho_3 + \rho_4) - k_{+2} - k_{+1}. \tag{A7}$$

Thus, we have shown that the three rate constants are uniquely identifiable from the data. We wish to point out that we are not guaranteed unique identifiability from the above four equations in three unknowns since the equations are nonlinear. In practice we program Eqs. A1–A3 and make the rate constants the only free parameters in the optimization routine. This is preferable to using an equation of the form of A4 because A4 has an additional free parameter. An additional advantage is that many parameter estimation routines will then provide confidence intervals on the parameters of interest.

The waiting time PDF P_{RO} (Patlak and Horn, 1982; Colquhoun and Hawkes, 1981) is given by

$$P_{\mathrm{RO}} = \frac{\rho_3\rho_4}{\rho_4 - \rho_3} e^{-\rho_3 t} - \frac{\rho_3\rho_4}{\rho_4 - \rho_3} e^{-\rho_4 t}, \tag{A8}$$

where ρ_3 and ρ_4 are defined above (Eqs. A2 and A3). Note that in Eq. A8 only two parameters appear. Thus, in this case if we fit the data with Eq. A8 we would obtain two equations relating quantities in A8 to the three rate constant parameters of interest. Thus, an infinite number of rate constants would satisfy the equations, and the rate constants are not identifiable from the waiting time distribution.

The apparent burst length PDF (Colquhoun and Hawkes, 1981) is given by

$$P_{\mathrm{bu}} = \frac{\rho_1\rho_2}{(\rho_2 - \rho_1)(k_{+2} + k_{-1})}[(k_{+2} + k_{-1} - \rho_1)e^{-\rho_1 t} + (\rho_2 - k_{+2} - k_{-1})e^{-\rho_2 t}] \tag{A9}$$

where

$$\rho_1,\ \rho_2 = 0.5[b \pm (b^2 - 4c)^{0.5}] \tag{A10}$$

and

$$b = k_{-2} + k_{+2} + k_{-1}$$
$$c = k_{-2}k_{-1}. \tag{A11}$$

From analyses similar to those above, it can be shown that k_{-1}, k_{+2}, and k_{-2} are identifiable from the apparent burst duration data. The last distribution that is normally considered is the open time distribution. The trivial result here is that k_{-2} is identifiable from the open time distribution.

We should note that identifiability as we use it here says nothing about the properties of the data. Identifiability is purely a mathematical concept. When working with real data, the best parameter estimates are obtained from the global minimum of the objective function, or the minimum over the entire parameter space. Local minima of the same value would lead to non-unique parameter estimates even if an analysis such as that above indicated that the parameters were uniquely identifiable.

APPENDIX B

Analysis of the Time and Amplitude of the Peak of the Waiting Time PDF

The equation for the waiting time of a three-state, sequential model is given by Colquhoun and Hawkes (1981):

$$P_{RO} = \frac{\rho_3\rho_4}{\rho_3 - \rho_4}(e^{-\rho_4 t_R} - e^{-\rho_3 t_R}), \tag{B1}$$

where ρ_3 and ρ_4 are given in Eqs. A2 and A3.

Eq. B1 has a maximum that occurs at time t_p and we find it by differentiating Eq. B1, setting the result to zero, and solving for t_p. We quickly obtain

$$\frac{\rho_3}{\rho_4} = e^{-t_p(\rho_4 - \rho_3)}, \tag{B2}$$

and after rearrangement we have

$$t_p = \frac{\ln(\rho_3/\rho_4)}{\rho_3 - \rho_4}. \tag{B3}$$

We now wish to find the value of the maximum. We insert Eq. B3 into B1 and after considerable rearrangement obtain

$$P_{RO}(t_p) = \rho_4\left(\frac{\rho_4}{\rho_3}\right)^{\frac{\rho_4}{\rho_3 - \rho_4}}. \tag{B4}$$

Using Eqs. B2 and B4 we get

$$P_{RO}(t_p) = \rho_4 e^{-\rho_4 t_p} = \rho_3 e^{-\rho_3 t_p} = f(\rho). \tag{B5}$$

In Eq B5, $f(\rho)$ is the maximum value of the waiting time PDF, and it is plotted in Fig. 8*A* as a function of ρ with $t_p = 1.0$ ms. Note that given a waiting time histogram with a peak at 1 ms and the amplitude of the peak, we can obtain the ρ values from this curve. Depending on the value of the peak we can obtain two ρ values corresponding to ρ_3 and ρ_4, or at the peak of this function we would get two ρ's of value ρ_p, corresponding to a repeated eigenvalue of the system.

We wish also to investigate the maximum amplitude permissible from this PDF. From the results above, this should occur in the case of redundant roots, i.e., $\rho_p = B/2$ from

Eqs. A2 and A3. In this case, Eq. B1 is no longer valid, and we must solve the set of differential equations once again for the case of a repeated root given by $\rho_p = B/2$. The result is

$$P_{RO}^*(t) = \frac{B^2}{4} te^{-Bt/2}. \tag{B6}$$

We now find the maximum value of this function as a function of time. The peak occurs at

$$t_p^* = \frac{2}{B} \tag{B7}$$

and the value at the peak is given by

$$P_{RO}^*(t_p) = \frac{1}{t_p e}. \tag{B8}$$

Eq. B8 thus yields the maximum obtainable value of the waiting time PDF as a function of the time of the peak. Measured values must be less than or equal to this function and should fall in the shaded region of Fig. 8. Note that all but one of the data points fall outside the acceptable region, which indicates an inconsistency with the model.

Supported in part by National Institutes of Health grant NS-11453. Dr. Brown is a Josiah Macy Fellow.

Received for publication 3 June 1983 and in revised form 19 December 1983.

REFERENCES

Bevington, P. R. 1969. Data Reduction and Error Analysis for the Physical Sciences. McGraw-Hill, New York. 336 pp.

Brehm, P., and R. Eckert. 1978. Calcium entry leads to inactivation of calcium channel in *Paramecium. Science (Wash. DC).* 202:1203–1206.

Brown, A. M., H. Camerer, D. L. Kunze, and H. D. Lux. 1982. Similarity of calcium current in three different species. *Nature (Lond.).* 299:156–158.

Brown, A. M., K. Morimoto, Y. Tsuda, and D. L. Wilson. 1981. Ca current-dependent and voltage-dependent inactivation in calcium channels in *Helix Aspersa. J. Physiol. (Lond.)* 320:193–218.

Brown, A. M., Y. Tsuda, and D. L. Wilson. 1983. A description of activation and conduction in calcium channels based on tail and turn-on current measurements. *J. Physiol. (Lond.).* 344:549–583.

Brown, R. F. 1980. Compartmental systems analysis: state of the art. *IEEE Trans. Biomed. Eng.* BME-27:1–11.

Cachelin, A. B., J. E. dePeyer, S. Kokubun, and H. Reuter. 1983. Ca channel modulation by 8-bromocyclic AMP in cultured heart cells. *Nature (Lond.).* 304:462–464.

Cobelli, C., and J. J. DiStefano. 1980. Parameter and structural identifiability concepts and ambiguities: a critical review and analysis. *Am. J. Physiol.* 239:R7–R24.

Colquhoun, D., and A. G. Hawkes. 1977. Relaxation and fluctuations of membrane currents that flow through drug-operated channels. *Proc. R. Soc. Lond. B Biol. Sci.* 199:231–262.

Colquhoun, D., and A. G. Hawkes. 1981. On the stochastic properties of single ion channels. *Proc. R. Soc. Lond. B Biol. Sci.* 211:205–235.

Dionne, V. E., and M. D. Liebowitz. 1982. Acetylcholine receptor kinetics: a description from single-channel currents at snake neuromuscular junctions. *Biophys. J.* 39:253–261.

Fenwick, E. M., A. Marty, and E. Neher. 1982. Sodium and Ca channels in bovine chromaffin cells. *J. Physiol. (Lond.).* 331:599–636.

Hagiwara, S., and H. Ohmori. 1983. Studies of single calcium channel currents in rat clonal pituitary cells. *J. Physiol. (Lond.).* 336:649–661.

Jennrich, R. I., and M. L. Ralston. 1979. Fitting nonlinear models to data. *Annu. Rev. Biophys. Bioeng.* 8:195–238.

Kormylo, J. J., and V. K. Jain. 1974. Two-pass recursive digital filter with zero phase shift. *IEEE Trans. Acoust. Speech Signal Process.* ASSP-22:384–387.

Lowry, T. M., and W. T. John. 1910. Studies of dynamic isomerism. XII. The equations for two consecutive unimolecular changes. *J. Chem. Soc.* 97:2634–2645.

Lux, H. D., and A. M. Brown. 1984. Patch and whole cell calcium currents recorded simultaneously in snail neurons. *J. Gen. Physiol.* 83:727–750.

Lux, H. D., and K. Nagy. 1981. Single channel Ca^{++} currents in *Helix pomatia* neurons. *Pflügers Arch. Eur. J. Physiol.* 391:252–254.

Marquardt, D. W. 1963. An algorithm for least-square estimation of non-linear parameters. *J. Ind. Appl. Math.* 11:431–441.

Patlak, C. S., and R. Horn. 1982. Effect of *N*-bromoacetamide on single sodium channel currents in excised membrane patches. *J. Gen. Physiol.* 79:333–352.

Reuter, H., C. F. Stevens, R. W. Tsien, and G. Yellen. 1982. Properties of single calcium channels in cardiac cell culture. *Nature (Lond.).* 297:501–504.

Yatani, A., D. L. Wilson, and A. M. Brown. 1983. Recovery of Ca currents from inactivation: the roles of Ca influx, membrane potential, and cellular metabolism. *Cell. Mol. Neurobiol.* 3:381–395.